JACC: BASIC TO TRANSLATIONAL SCIENCE VOL. 8, NO. 12, 2023

ORIGINAL RESEARCH - PRECLINICAL

Mesenchymal Stromal Cell Delivery Via Cardiopulmonary Bypass Provides Neuroprotection in a Juvenile Porcine Model

Kamil Sarkislali, MD,[a,b,*] Kei Kobayashi, MD, PhD,[a,b,c,*] Nemanja Sarić, PhD,[a,b,*] Takuya Maeda, MD, PhD,[a,b] Soichiro Henmi, MD, PhD,[a,b,c] Fahad A. Somaa, PhD,[a,b] Ankush Bansal, PhD,[a] Shao Ching Tu, MD,[a,b] Camille Leonetti, PhD,[a,b] Chao-Hsiung Hsu, PhD,[d] Jingang Li, MD, PhD,[a,b] Pranav Vyas, MD,[e,f] Yuka Imamura Kawasawa, PhD,[g] Tsang-Wei Tu, PhD,[d] Paul C. Wang, PhD,[d,h] Patrick J. Hanley, PhD,[f,i] Kazue Hashimoto-Torii, PhD,[a,f,j] Joseph A. Frank, MD, MS,[k,l] Richard A. Jonas, MD,[a,b,c,f] Nobuyuki Ishibashi, MD[a,b,c,f,j]

VISUAL ABSTRACT

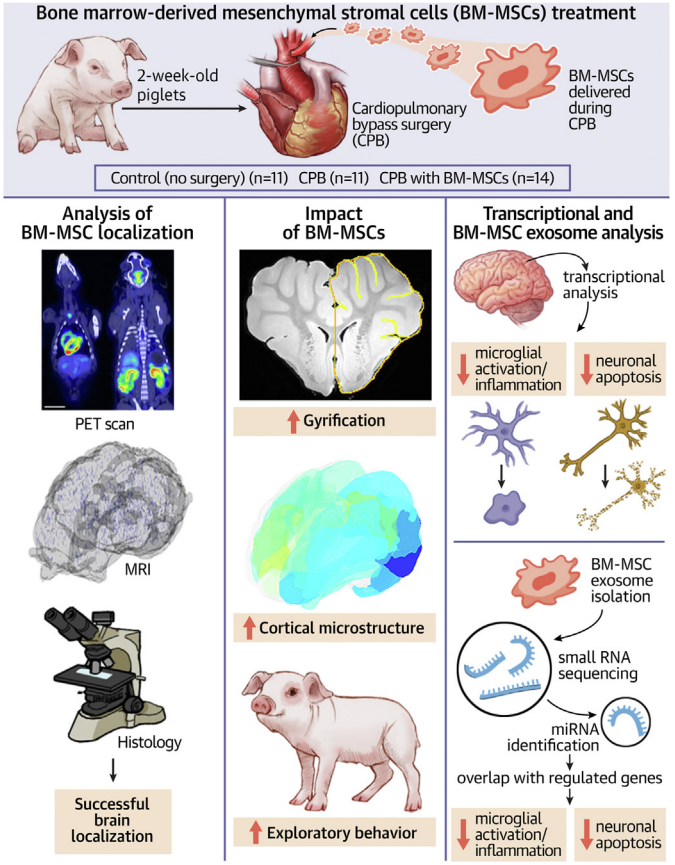

Sarkislali K, et al. J Am Coll Cardiol Basic Trans Science. 2023;8(12):1521-1535.

HIGHLIGHTS

- **Oxidative and inflammatory stresses attributable to cardiopulmonary bypass cause prolonged microglia activation and cortical dysmaturation in the neonatal and infant brain, thereby contributing to neurodevelopmental impairments in children with congenital heart disease.**
- **This study using our translational piglet model found that delivery of mesenchymal stromal cells via cardiopulmonary bypass minimizes microglial activation and neuronal apoptosis, with subsequent improvement of cortical dysmaturation and behavioral alteration after neonatal cardiac surgery.**
- **Transcriptomic analyses suggest that exosome-derived miRNAs such as miR-21-5p may be the key drivers of suppressed apoptosis and STAT3-mediated microglial activation observed following infusion of mesenchymal stromal cells.**
- **Successful completion of a phase 1 trial will be required to design new cell-based approaches for improvement of neuro-developmental impairments in children with congenital heart disease.**

ISSN 2452-302X https://doi.org/10.1016/j.jacbts.2023.07.002

JACC: BASIC TO TRANSLATIONAL SCIENCE VOL. 8, NO. 12, 2023
DECEMBER 2023:1521–1535

ABBREVIATIONS AND ACRONYMS

BM-MSC = bone marrow-derived mesenchymal stromal cell

CHD = congenital heart disease

CPB = cardiopulmonary bypass

DEG = differentially expressed gene

FA = fractional anisotropy

IPA = Ingenuity Pathway Analysis

JAK = Janus kinase

miRNA = microRNA

MRI = magnetic resonance imaging

NF-κB = nuclear factor-κB

SPIO = superparamagnetic iron oxide

STAT = signal transducer and activator of transcription

TF = transcription factor

WM = white matter

SUMMARY

Oxidative/inflammatory stresses due to cardiopulmonary bypass (CPB) cause prolonged microglia activation and cortical dysmaturation, thereby contributing to neurodevelopmental impairments in children with congenital heart disease (CHD). This study found that delivery of mesenchymal stromal cells (MSCs) via CPB minimizes microglial activation and neuronal apoptosis, with subsequent improvement of cortical dysmaturation and behavioral alteration after neonatal cardiac surgery. Furthermore, transcriptomic analyses suggest that exosome-derived miRNAs may be the key drivers of suppressed apoptosis and STAT3-mediated microglial activation. Our findings demonstrate that MSC treatment during cardiac surgery has significant translational potential for improving cortical dysmaturation and neurological impairment in children with CHD.

Many children with congenital heart disease (CHD) experience a wide range of neurologic impairments[1,2]; however, few treatment options are available. The etiology is cumulative and multifactorial, including genetic predisposition and altered fetal cerebral circulation.[1,3] Additionally, oxidative stress and systemic inflammation during cardiac surgery remain major pathologic events in the neonatal and infant brain.[4] Our previous studies found prolonged microglia expansion and cortical dysmaturation after cardiopulmonary bypass (CPB).[5,6] Newly acquired brain damage is commonly recognized after surgery with current technologies.[7,8] Thus, further refinement of pediatric cardiac surgery will likely assist in the improvement of neurodevelopmental outcomes in CHD.

Bone marrow–derived mesenchymal stromal cells (BM-MSCs) possess extensive anti-inflammatory and immunomodulatory properties.[9-11] Notably, MSC-derived therapies have been studied in multiple clinical trials, including in neonates and infants.[12] We hypothesized that BM-MSC delivery to the early postnatal brain at the time of cardiac surgery inhibits neuronal damage through the suppression of inflammatory reactions.

Intravenous cell injection causes high accumulation of cells primarily in the lungs.[13,14] In contrast, intra-arterial infusion results in a higher percentage of MSCs localizing to the damaged brain.[15,16] CPB represents a unique intervention in infants with CHD because the brain is perfused under controlled flow. CPB also allows intra-arterial transfusion of BM-MSCs into the ascending aorta through arterial cannulation. These conditions led to our proposal of using CPB itself as a delivery system of MSCs into the systemic circulation, including the cerebral circulation of the infant brain. By leveraging cellular/molecular, imaging, and behavioral approaches in the piglet CPB model, the current study assessed the neuroprotective effects of BM-MSC delivery through CPB.

METHODS

EXPERIMENTAL MODEL. This study involved a total of 61 Yorkshire pigs (experimental piglets: n = 36;

From the [a]Center for Neuroscience Research, Children's National Hospital, Washington, DC, USA; [b]Sheikh Zayed Institute for Pediatric Surgical Innovation, Children's National Hospital, Washington, DC, USA; [c]Children's National Heart Institute, Children's National Hospital, Washington, DC, USA; [d]Molecular Imaging Laboratory, Department of Radiology, Howard University, Washington, DC, USA; [e]Department of Radiology, Children's National Hospital, Washington, DC, USA; [f]Department of Pediatrics, George Washington University School of Medicine and Health Sciences, Washington, DC, USA; [g]Departments of Pharmacology and Biochemistry and Molecular Biology, Institute for Personalized Medicine, Penn State College of Medicine, Hershey, Pennsylvania, USA; [h]Department of Electrical Engineering, Fu Jen Catholic University, New Taipei City, Taiwan; [i]Program for Cell Enhancement and Technologies for Immunotherapy, Division of Blood and Marrow Transplantation, Center for Cancer and Immunology Research, Children's National Hospital, Washington, DC, USA; [j]Pharmacology and Physiology, George Washington University School of Medicine and Health Sciences, Washington, DC, USA; [k]Frank Laboratory, Radiology and Imaging Sciences, National Institutes of Health; Bethesda, Maryland, USA; and the [l]National Institute of Biomedical Imaging and Bioengineering, National Institutes of Health, Bethesda, Maryland, USA. *Drs Sarkislali, Kobayashi, and Sarić contributed equally to this work.
The authors attest they are in compliance with human studies committees and animal welfare regulations of the authors' institutions and Food and Drug Administration guidelines, including patient consent where appropriate. For more information, visit the Author Center.

Manuscript received February 2, 2023; revised manuscript received June 13, 2023, accepted July 5, 2023.

blood donor pigs: n = 25). Piglets at 2 weeks of age were randomly assigned to 3 groups: 1) control (no surgery; n = 11); 2) CPB (n = 11); and 3) CPB with BM-MSC administration during the rewarming period (CPB + MSC; n = 14). Naive control was used to compare the effect of BM-MSC treatment to the overall impact of cardiac surgery with CPB. CPB was established via ascending aortic perfusion and right atrial drainage. BM-MSCs were manufactured from human bone marrow using the methods used for clinical trials at Children's National Hospital (Pro000006717; STOMP [Safety and Tolerability of Allogeneic Mesenchymal Stromal Cells in Pediatric and Adult Inflammatory Bowel Disease], Pro000011914; MeDCaP [Mesenchymal Stromal Cells Delivery through Cardiopulmonary Bypass in Pediatric Cardiac Surgery]) (Supplemental Figures 1A to 1C).[17] Either phosphate-buffered saline or phosphate-buffered saline with BM-MSCs (1×10^7 cells/kg) was delivered through CPB (Supplemental Figure 1D). Positron emission tomography was performed at 1 hour after BM-MSC delivery. Magnetic resonance imaging (MRI) and cellular/molecular assessments were performed at either 3 hours or 4 weeks after CPB. Neurologic and behavioral outcomes were assessed up to 4 weeks. Immunohistochemistry was performed using coronal sections from the frontal cortex (Supplemental Figure 1E). Total RNA was extracted from premotor cortices and subjected to RNA sequencing. We performed all experiments in compliance with the National Institutes of Health "Guide for the Care and Use of Laboratory Animals." The study was approved by the Animal Care and Use Committee of the Children's National Hospital.

STATISTICAL ANALYSIS. The data distributions are presented as mean ± SD or box-and-whisker plots from minimum to maximum. The Shapiro-Wilk test was used to test if continuous data were normally distributed. Student's *t*-test was performed to compare continuous variables between 2 groups. One-way analysis of variance with the Bonferroni post hoc test was used to evaluate multiple pairwise comparisons among >2 groups. We applied 2-way repeated-measures analysis of variance with either time or brain region as a fixed effect for cellular/molecular, structural, and behavioral analyses. The Spearman rank correlation coefficient (r_s) was used to evaluate the relationship between 2 variables. If continuous variables demonstrated a significant departure from normality, we applied nonparametric methods. *P* values of <0.05 were considered statistically significant.

Detailed methods are described in the Supplemental Appendix.

RESULTS

CPB IS AN EFFICIENT ADMINISTRATION SYSTEM FOR BM-MSC DELIVERY INTO THE DEVELOPING BRAIN. BM-MSCs have been widely applied for neural repair and regeneration.[10-12] However, the migration dynamics of BM-MSCs delivered through CPB have never been determined. To assess the whole-body distribution of BM-MSCs, cells were labeled with ^{18}F-fluorodeoxyglucose and delivered through CPB (**Figure 1A**). Results from our positron emission tomography study indicated that intra-arterial delivery via CPB uniformly distributed BM-MSCs to most of the organs analyzed, including brain, heart, and kidney (**Figures 1B and 1C**). The lungs and intestine showed lower uptake (**Figure 1C**), demonstrating a unique distribution of BM-MSCs after administration through CPB.

We next used an MRI-based cell-tracking technique with superparamagnetic iron oxide (SPIO) nanoparticles to define the destinations of BM-MSCs in the brain. Efficient uptake of SPIOs into BM-MSCs was indicated by the fluorescent tag associated with SPIOs (Supplemental Figure 2A). SPIOs neither damage cells nor change their behavior in a variety of assayed cell types.[18] Consistent with previous findings, there were no alterations in the differentiation properties of BM-MSCs after SPIO labeling (Supplemental Figures 2B and 2C). At 3 hours after CPB, T2*-weighted imaging showed diffuse distribution of hypointense voxels (ie, SPIO particles) throughout the entire brain (**Figure 1D**). An even ratio of SPIO signals within the right and left hemispheres was revealed (Supplemental Figure 2D). When the brain was subdivided, there were no differences in the number and percentage of SPIO particles (Supplemental Figures 2E and 2F). On the other hand, the density of SPIO particles was higher in the cerebellum and deep white matter (WM) compared with the posterior cortex (**Figure 1E**). Following brain damage, MSCs can migrate toward an injured site through the SDF-1/CXCR4 pathway.[19] In our previous studies, cerebellar Purkinje cells were more susceptible to CPB-induced inflammation than other cell populations.[20]

Because SPIO-particles co-label with a green fluorescence, SPIO-labeled BM-MSCs were further analyzed histologically. SPIO particles are passive contrast agents. Indeed, 44% of SPIO particles were not incorporated by human nuclear antibody$^+$ BM-MSCs (Supplemental Figures 3A and 3B). On the

FIGURE 1 CPB Is an Efficient Cell Delivery System Into the Brain

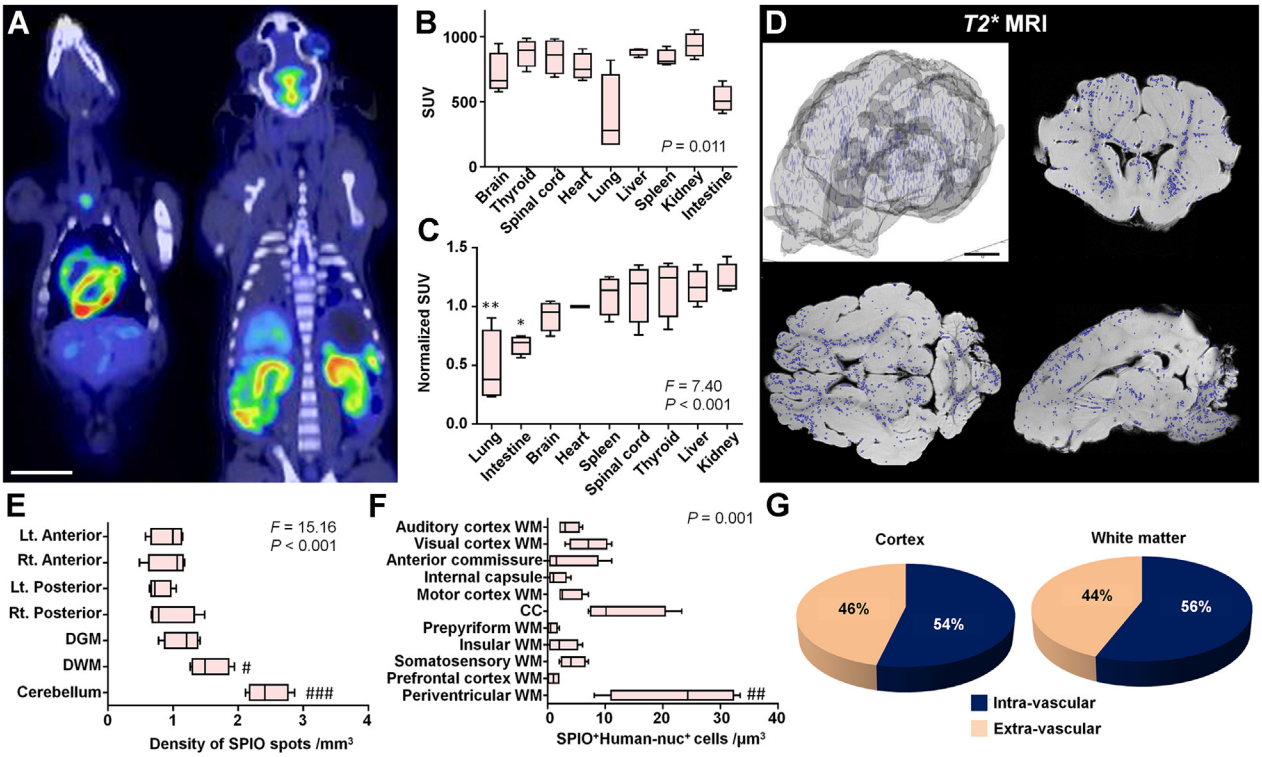

(A) Positron emission tomography imaging. Scale bar: 5 cm. (B, C) ^{18}F-fluorodeoxyglucose uptakes within organs quantified (B) with SUV normalized to body weight and (C) with normalized SUV dividing by the value of heart. (D) T2*-weighted MRI. Scale bar: 10 mm. (E) The density of hypointense signals. (F, G) Distribution of human nuclear$^+$SPIO$^+$ bone marrow–derived mesenchymal stromal cells within each WM region and between (F) intravascular and (G) extravascular spaces. Data are shown as box-and-whisker plots from minimum to maximum (n = 4 each). *P* values were determined by 1-way analysis of variance with (C, E) Bonferroni comparisons and (B, F) the Kruskal-Wallis test with Dunn's comparisons. *$P < 0.05$ vs liver and kidney. **$P < 0.05$ vs thyroid gland, spinal cord, heart, liver, spleen, and kidney. $^{\#}P < 0.05$ vs Lt. posterior. $^{\#\#}P < 0.05$ vs prefrontal and prepyriform WM. $^{\#\#\#}P < 0.001$ vs Lt. and Rt. anterior and Lt. and Rt. posterior. CC = corpus callosum; DGM = deep gray matter; DWM = deep white matter; Lt. = left; MRI = magnetic resonance imaging; Rt. = right; SPIO = superparamagnetic iron oxide; SUV = standardized-uptake value; WM = white matter.

other hand, 76% of BM-MSCs were labeled with SPIO particles (Supplemental Figure 3C). When human nuclear antibody$^+$SPIO$^+$ BM-MSCs were analyzed, we found an even distribution of delivered BM-MSCs in cortex and WM (Supplemental Figure 3D). In our previous studies, periventricular WM and corpus callosum were more vulnerable to CPB-induced brain insults compared with other WM regions.[21] Although there were no differences in the cell number between 11 cortical areas (Supplemental Figure 3E), an increase in the number of BM-MSCs was identified in periventricular WM followed by corpus callosum (**Figure 1F**). Notably, BM-MSCs were not only located within the vasculature (Supplemental Figure 3F) but also migrated into the extravascular space. Respectively, 46% and 44% of BM-MSCs were found in parenchyma in the cortex and WM (**Figure 1G**). Together, our results indicate that CPB is an efficient system for administering BM-MSCs into the developing brain.

When we analyzed the broad systemic effects of BM-MSC delivery during CPB, there were no differences in operative conditions (Supplemental Table 1). In addition, we did not observe allergic reactions and significant detrimental changes in clinically relevant biomarkers at 3 hours post-CPB (Supplemental Table 2). Consistent with previous findings demonstrating the safety of intra-arterial cell infusion after stroke,[22,23] we have not observed any signs of stroke by MRI (Supplemental Figure 4) or ischemic damage by immunohistochemistry (ie, accumulation or clustering of caspase3$^+$ cells and iba1$^+$ microglia) after

FIGURE 2 **Bone Marrow-Derived Mesenchymal Stromal Cell Delivery Suppresses Microglial STAT3 Phosphorylation, Thereby Inhibiting Its Activation**

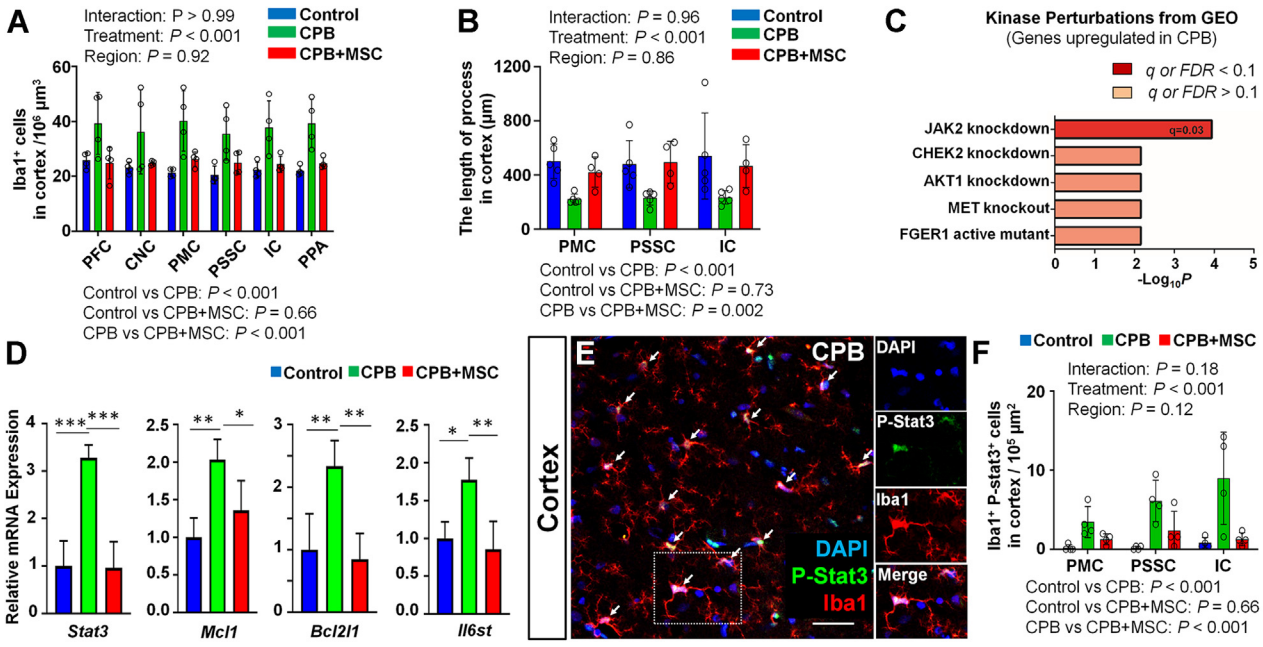

(A) The number of Iba1$^+$ cortical microglia. (B) The length of cortical microglia processes. (C) JAK2 as the top predicted kinase whose knockdown leads to the down-regulation of genes found up-regulated after CPB. (D) Relative mRNA expression. (E) Phosphorylated Stat3 with Iba1 in cortex after CPB. Scale bar: 50 µm. (F) The number of Iba1$^+$P-Stat3$^+$ cells in cortex. Data are shown as mean ± SD (n = 4 or 5 each). *P* values were determined by (D) 1-way analysis of variance and (A, B, F) 2-way analysis of variance with Bonferroni comparisons. *$P < 0.05$, **$P < 0.01$, ***$P < 0.001$. CNC = cingulate cortex; CPB = cardiopulmonary bypass; DAPI = 4′,6-diamidino-2-phenylindole; FDR = false discovery rate; IC = insular cortex; mRNA = messenger RNA; MSC = mesenchymal stromal cell; PFC = prefrontal cortex; PMC = premotor cortex; PPA = prepyriform area; P- = phosphorylated; PSSC = primary somatosensory cortex; STAT = signal transducer and activator of transcription.

BM-MSC delivery. Altogether, our studies demonstrate that BM-MSC delivery through CPB at the time of surgery should be safe and feasible in children with CHD.

BM-MSC TREATMENT REDUCES MICROGLIA EXPANSION AND MODULATES THEIR ACTIVATION STATE RESULTING FROM CPB. Rapid responses of microglia cells to brain injury have been well characterized.[24] Consistent with the findings, increases in Iba1$^+$ microglia were identified at 3 hours after CPB in 6 cortical and 5 WM regions (**Figure 2A**, Supplemental Figures 5A and 5B). Notably, the CPB-induced acute increase in microglia cells was suppressed after BM-MSC infusion (**Figure 2A**, Supplemental Figures 5A and 5B). There were no differences in Iba1$^+$ cell numbers between the control and CPB + MSC groups (**Figure 2A**, Supplemental Figure 5B), suggesting that BM-MSC treatment normalizes CPB-induced acute microglial increases.

BM-MSCs regulate microglial activation and participate in the phenotypic switch from a proinflammatory to repair-permissive state.[10] When we assessed the activation status by CD11b immunoreactivity, CPB caused an increase in CD11b$^+$Iba1$^+$ cells compared to control (Supplemental Figures 5A, 5C, and 5D). The number of CD11b$^+$ microglia after BM-MSC treatment was lower than in CPB (Supplemental Figures 5A, 5C, and 5D). In contrast to their ramified morphology under normal conditions, activated microglia undergo structural remodeling and adopt an amoeboid morphology with highly retracted processes.[24] In both cortex and WM, CPB caused decreases in the total length and branch number of microglial processes compared to control (**Figure 2B**, Supplemental Figures 6A to 6D). Consistent with our findings using the integrin marker CD11b, BM-MSC treatment inhibited the CPB-induced morphologic alterations (**Figure 2B**, Supplemental Figures 6A to 6D). Brain region was not a factor in the impact of BM-MSCs (**Figures 2A and 2B**, Supplemental Figures 6A to 6D), indicative of a pan-cerebral effect. The results indicate that BM-MSCs delivered through CPB shift the state of microglial activation resulting from cardiac surgery.

BM-MSC DELIVERY SUPPRESSES MICROGLIAL SIGNAL TRANSDUCER AND ACTIVATOR OF TRANSCRIPTION 3 PHOSPHORYLATION CAUSED BY CPB, THEREBY INHIBITING ITS ACTIVATION. To further characterize the molecular events occurring during CPB-induced oxidative and inflammatory stresses, genome-wide RNA profiling was performed. Our analysis revealed 303 differentially expressed genes (DEGs) at 3 hours post-CPB (229 up-regulated, 74 down-regulated) (Supplemental Figures 7A and 7B). We focused on subsetted down-/up-regulated DEG lists for ontology analyses to detect biologically meaningful patterns. Within the list, CPB up-regulated caspase 8 (*Casp8*) and apoptotic chromatin condensation inducer 1 (*Acin1*) (Supplemental Figure 7C), which encode upstream/downstream effectors of the extrinsic apoptotic signaling pathway.

Gene ontology analyses were also performed to predict transcription factors (TFs) by binding motifs/sites detected in promoters of genes up-regulated by CPB. The analysis identified TP53 as the top predicted TF (Supplemental Figure 7D), suggesting a likely role for p53 activation after CPB. When we assessed overlap between CPB-induced up-regulated genes and DEGs after TF loss-of-function mutations, heat shock factor 1 (HSF1) was the top predicted factor whose loss of function induced similar gene expression changes to CPB (Supplemental Figure 7E, Supplemental Table 3).

We also tested for overlap between genes up-regulated by CPB and DEGs after various TF genetic manipulations obtained from the Gene Expression Omnibus database. Statistically significant fractions of CPB-induced up-regulated genes were found down-regulated after *Tp53* and/or *Stat3* in silico knockdown (Supplemental Figure 7F, Supplemental Table 3), suggesting that the same gene sets that were identified as up-regulated after CPB are also up-regulated after p53/signal transducer and activator of transcription (STAT) 3 pathway activation. Finally, our gene set enrichment analysis revealed Janus kinase (JAK) 2 as the top predicted kinase for which in silico knockdown leads to the down-regulation of genes found up-regulated after CPB (**Figure 2C**, Supplemental Table 3), indicating a likely activation signature of JAK2-STAT3 signaling after CPB. Together, our transcriptomic profiling revealed links between CPB-induced brain insults and the activation of p53 and JAK2-STAT3 pathways, both of which are known to be critical in oxidative stress and inflammatory responses as well as cell survival.

Consistent with our transcriptomic evidence and functional ontology data, we identified significant increases in *Stat3*, *Bcl2l1*, *Mcl1*, and *IL6st* transcripts in the frontal cortex after CPB (**Figure 2D**). *Il6st* is required for JAK activation, which in turn leads to STAT3 activation. Both *Bcl2l1* and *Mcl1* are known STAT3 target genes. Microglial STAT3 phosphorylation plays a critical role in microglia activation and subsequent inflammatory response.[25,26] Indeed, CPB caused an increase in phosphorylated STAT3^{+} microglial cells (**Figures 2E and 2F**). Notably, BM-MSC delivery suppressed CPB-induced microglial STAT3 phosphorylation (**Figure 2F**). In addition, BM-MSC treatment inhibited the expression of *Stat3*, *Bcl2l1*, *Mcl1*, and *IL6st* transcripts caused by CPB (**Figure 2D**). Finally, STAT3 phosphorylation was correlated with proinflammatory morphologic changes in microglial processes (Supplemental Figures 7G and 7H), suggesting a significant link between STAT3 phosphorylation and microglial activation after CPB. Altogether, our results indicate that BM-MSC delivery during CPB suppresses STAT3 phosphorylation and transcript levels in microglia cells, thereby reducing their activation after cardiac surgery.

BM-MSC DELIVERY DURING CPB INHIBITS NEURONAL APOPTOSIS AFTER CARDIAC SURGERY. In addition to microglia activation, CPB caused significant increases in caspase 3^{+} cells in both upper and lower cortical layers (Supplemental Figures 8A and 8B). Consistent with acute caspase 3 activation after traumatic neuronal injury,[27] caspase 3 was activated at 3 hours but not at 1 day after CPB (Supplemental Figures 8C and 8D). Notably, following BM-MSC treatment, CPB-induced caspase activation was inhibited in both cortical layers (Supplemental Figures 8A and 8B). Additionally, BM-MSC treatment reduced the number of caspase3^{+}NeuN^{+} neurons (**Figure 3A**, Supplemental Figures 9A to 9C). After CPB, 40% of cortical neurons displayed activated caspase 3 (**Figure 3B**). BM-MSC delivery normalized the caspase 3 activation (**Figure 3B**, Supplemental Figure 9D). Consistent with the findings, CPB-induced increases in TUNEL^{+}-apoptotic neurons were inhibited after BM-MSC treatment in thr3ee different cortical regions and both upper and lower layers (**Figure 3C**, Supplemental Figures 9E and 9F), indicating MSC-induced inhibition of neuronal apoptosis after CPB.

Our transcriptomic profiling comparing the CPB and CPB + MSC groups identified various DEGs related to regulation of the intrinsic mitochondria-dependent apoptotic pathway and mitochondrial integrity (**Figure 3D**, Supplemental Figure 10A). Genes found down-regulated by BM-MSC treatment included *Nfkbia* and *Bad*, encoding an inhibitory subunit of the nuclear factor κB (NF-κB) transcription factor (IκBα) and a proapoptotic *Bcl2* gene family

FIGURE 3 Bone Marrow-Derived MSCs Delivery During CPB Inhibits Neuronal Apoptosis After Cardiac Surgery

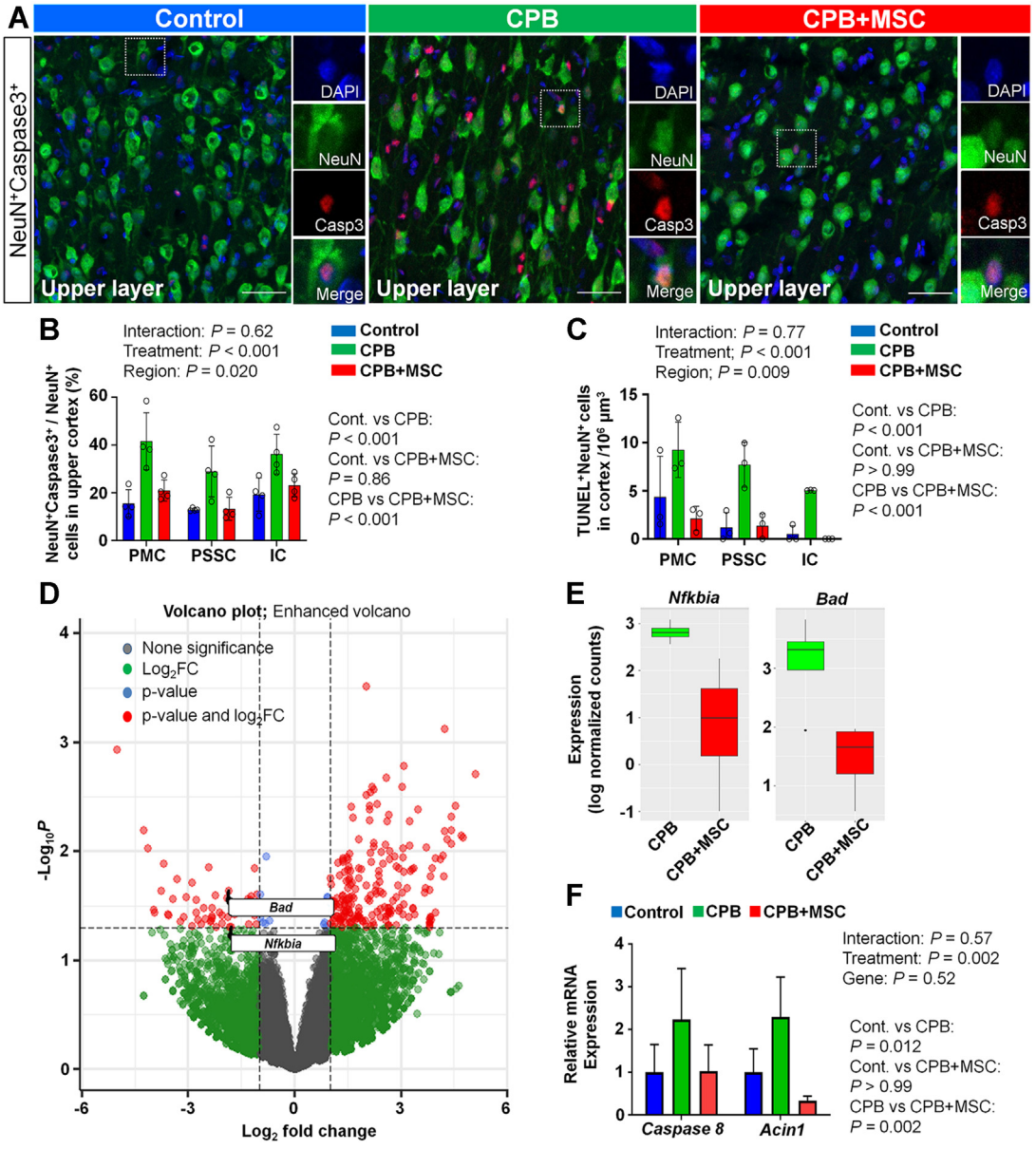

(A) NeuN$^+$caspase3$^+$ cells in the upper cortical layer. Scale bar: 50 µm. (B) The percentage of caspase3$^+$ neurons. (C) The number of NeuN$^+$TUNEL$^+$ cells. (D) Volcano plot showing genes differentially expressed between CPB and CPB + MSC cortex. (E) Normalized expression of *Nfkbia* and *Bad* in CPB vs CPB + MSC conditions. (F) Relative mRNA expression. Data are shown as mean ± SD (n = 4 or 5 each). (B, C, F) *P* values were determined by 2-way analysis of variance with Bonferroni comparisons. Cont. = control; FC = fold change; IC = insular cortex; PMC = premotor cortex; PSSC = primary somatosensory cortex; other abbreviations as in Figure 2.

(Figure 3E). Reduced expression of the IκBα subunit allows for nuclear translocation of NF-κB and enhanced cell survival because of antiapoptotic NF-κB signaling.[28] When we tested for in silico overlap between genes up-regulated by BM-MSC treatment and genes down-regulated after G protein-coupled receptor kinase genetic manipulations, RAF-1 in silico knockdown was identified as the top category (Supplemental Figure 10B), suggestive of BM-MSC-mediated promotion of RAF-1 signaling.

This finding is in agreement with the previously established role for RAF-1 signaling in suppressing apoptosis.[29] When we assessed overlap between genes down-regulated after BM-MSC treatment and DEGs after kinase enzyme genetic manipulations, MET (hepatocyte growth factor receptor) was identified as the top predicted receptor kinase whose knockout leads to up-regulation of genes found up-regulated after BM-MSC treatment (Supplemental Figure 10C), suggesting MSC-induced inhibition of the c-MET pathway signaling that is tightly interlinked with STAT3 activation.[30]

Overactivated microglia can promote neurotoxicity.[31] Apoptotic neurons are contacted by microglia expressing CD11b, which controls the production of microglial superoxide, thereby inducing neuronal death.[32] Indeed, BM-MSC delivery through CPB caused a decrease in CD11b expression on microglia (Supplemental Figure 5A, 5C, and 5D). When we assessed the relationship between neuronal apoptosis and microglial STAT3 activation, we found a positive correlation between caspase 3^+ neurons and the number of phosphorylated $STAT3^+$ cells (Supplemental Figure 11A). BM-MSCs can induce microglial phenotype switching to a less proinflammatory state, thereby protecting neuronal cells.[10,33] In consistence with this interpretation, there was a significant correlation between microglia activation, as defined by their morphology, and caspase activation in neurons (Supplemental Figures 11B and 11C).

Our transcriptomic profiling comparing control and CPB groups identified CPB-induced up-regulation of *Casp8* and *Acin1* (**Figure 2C**), genes encoding upstream/downstream effectors of the extrinsic apoptotic pathway. Consistent with these results, quantitative reverse transcription polymerase chain reaction analysis revealed a significant up-regulation in the expression of these effector genes after CPB (**Figure 3F**). In addition to a reduction in proapoptotic signaling and inhibition of neuronal apoptosis, BM-MSCs suppressed the expression of these transcripts (**Figure 3F**). Together, our results indicate that BM-MSC delivery during CPB reduces caspase activation in cortical neurons and inhibits the induction of apoptotic signals and neuronal apoptosis resulting from neonatal cardiac surgery.

BM-MSC TREATMENT IMPROVES THE POSTOPERATIVE COURSE AND BEHAVIORAL FUNCTION AFTER CARDIAC SURGERY. To assess whether the short-term cellular and molecular changes caused by BM-MSC treatment affect overall postoperative course and neurologic function, animals were assessed up to 4 weeks after surgery. T2*-weighted MRI showed no SPIO signals throughout the entire brain (**Figure 4A**). Diffusion-weighted imaging is highly sensitive to SPIO: however, we did not observe any image disturbance (**Figure 4B**), indicating no long-term residual BM-MSCs at 4 weeks post-CPB. Consistent with our findings in the acute period (Supplemental Figure 4), diffusion-weighted imaging displayed no signs of stroke and/or microembolism (**Figure 4B**). There were no differences in various biomarkers between groups (Supplemental Table 4). Altogether, our results from acute and survival studies support the safety of intra-arterial BM-MSC infusion through CPB.

There were no differences in body weights over time between groups (**Figure 4C**). When postoperative recovery was assessed, all animals were scored as fully recovered by postoperative day 7 (**Figure 4D**), consistent with our previous studies.[5,21] Notably, an improvement in overall recovery was revealed on day 2 after MSC treatment compared to CPB (**Figure 4D**). Open field tests can provide a simple and general measure of motor function and exploratory behaviors in this animal. Although there were no differences in open field locomotion (**Figures 4E and 4F**), significant differences in exploratory behaviors were displayed after surgery (**Figures 4G and 4H**). Following CPB, surgical animals displayed an increased duration of standing still and spent less time investigating compared to controls (**Figures 4G and 4H**), indicating reduced interest in exploring their test space. Notably, the CPB-induced behavioral alterations were alleviated by BM-MSC treatment (**Figure 4G**), particularly during the later time periods (standing still: $P = 0.030$ and $P = 0.049$ vs CPB at weeks 3 and 4, respectively; sniffing duration: $P = 0.044$ vs CPB at week 4), demonstrating MSC-induced improvements of the postoperative course and behavioral function after CPB.

BM-MSC TREATMENT MITIGATES STRUCTURAL ABNORMALITIES RESULTING FROM CPB. At 4 weeks after surgery, the overall brain weight after CPB was lower compared to controls (Supplemental Figure 12A). Our structural imaging analyses demonstrated differences in the volume of frontal cortices among the 3 groups (Supplemental Figure 12B), consistent with MSC-induced inhibition of neuronal apoptosis. Similar to our previous studies,[6] the gyrification index was lower after CPB compared to controls (**Figures 5A and 5B**). Notably, CPB-induced alterations of gyrification were improved in the brain with BM-MSC treatment (**Figures 5A and 5B**).

FIGURE 4 Bone Marrow–Derived MSC Treatment Improves Postoperative Course and Behavioral Alteration

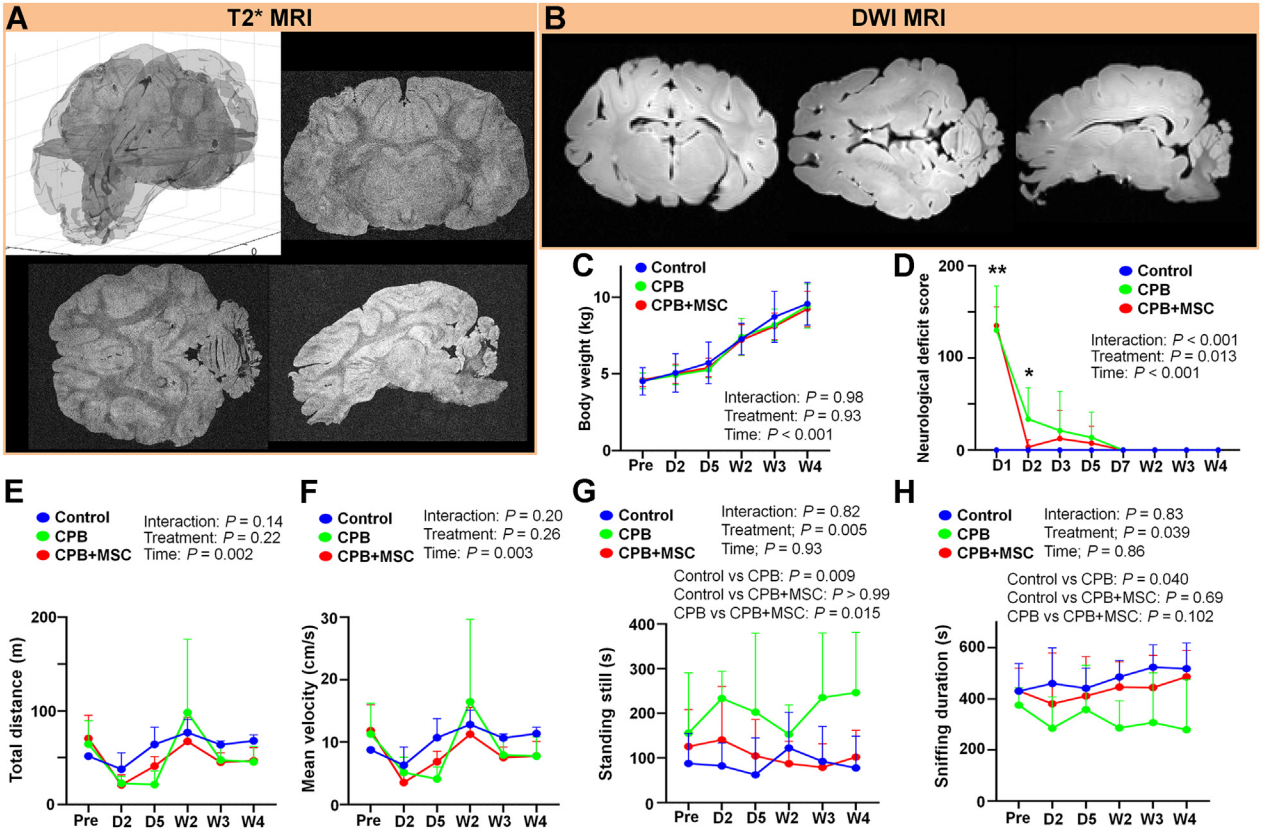

(A) T2*-weighted MRI. (B) DWI at 4 weeks post-CPB. (C) Change in body weight. (D) Changes in neurologic deficit score. (E, F) Changes in locomotion including (E) total distance moved and (F) velocity. (G, H) Changes in exploratory behaviors including (G) standing still duration and (H) sniffing duration. Data are shown as mean ± SD (n = 4-6 each). *P* values were determined by 2-way analysis of variance with Bonferroni comparisons. *$P < 0.05$ vs control and CPB + MSC, **$P < 0.001$ vs control. D = day; DWI = diffusion-weighted imaging; Pre = pretreatment; W = week; other abbreviations as in Figures 1 and 2.

To further assess cortical microstructure, high-resolution diffusion tensor imaging was used. Cortical FA after CPB was higher compared to control (**Figure 5C**), indicative of CPB-induced inhibition of the maturation-dependent decrease in cortical fractional anisotropy (FA).[34] Decreased mean diffusivity and radial diffusivity in the CPB group also indicated a loss of structural complexity in the developing cortex (**Figure 5D**, Supplemental Figure 13A). On the other hand, there were no differences in axial diffusivity among groups (Supplemental Figure 13B). Following BM-MSC infusion, we found a reduction in CPB-induced microstructural alterations, as determined by fractional anisotropy and radial diffusivity (**Figures 5C and 5D**). Together, our results indicate that BM-MSC treatment during CPB mitigates CPB-induced structural dysmaturation in the developing cortex.

BM-MSCs REDUCE PROLONGED MICROGLIA EXPANSION AND ACTIVATION IN CORTEX AFTER CARDIAC SURGERY. To assess the cellular events underlying the observed structural changes in the frontal cortex, we analyzed cortical neurons at postoperative week 4. Although there were differences in the cortical volumes (Supplemental Figure 12B), the density of neurons was similar among the 3 groups (Supplemental Figures 12C and 12D), suggesting an overall reduction of the number of cortical neurons. When we assessed whether the changes in microstructure determined by diffusion tensor imaging are associated with neuronal complexity,[34] there were no differences in the arborization complexity (Supplemental Figure 14). The results suggest that morphologic differences in pyramidal neurons are not a likely driver of microstructural changes after CPB. The presence of inflammation and gliosis could also

FIGURE 5 Bone Marrow-Derived MSC Treatment Mitigates Structural Abnormalities Resulting From CPB

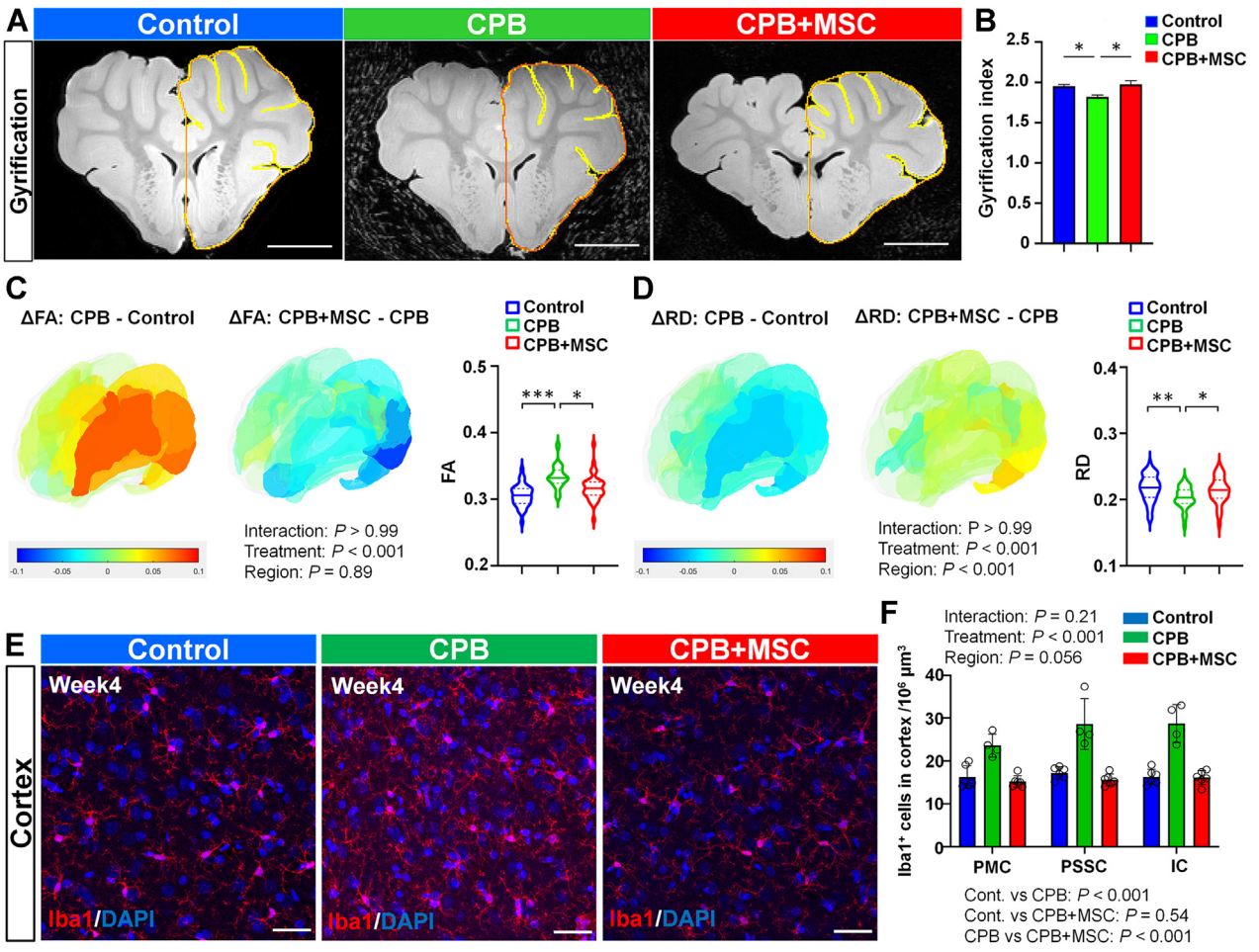

(A) Coronal sections of T2-weighted images. Scale bars = 1 cm. (B) Gyrification index expressed as a ratio of the inner vs outer perimeter traces (A). (C) Differences of cortical FA between CPB and control (left), CPB + MSC and CPB (center), and 3 groups (right). (D) Differences of cortical RD between CPB and control (left), CPB + MSC and CPB (center), and 3 groups (right). (E) Iba1$^+$ microglia in the cortex. Scale bar = 50 µm. (F) The number of Iba1$^+$ microglia. Data are shown as mean ± SD or violin plots with the median and quartiles (n = 4-6 each). *P* values were determined by (A) 1-way ANOVA and (C, D, F) 2-way ANOVA with Bonferroni comparisons. *$P < 0.05$, **$P < 0.01$, ***$P < 0.001$. AD = axial diffusivity; FA = fractional anisotropy; RD = radial diffusivity; other abbreviations as in Figures 1 to 4.

be one of the confounding factors that affect diffusion properties of brain tissues after injury.[35] Because BM-MSC treatment reduced acute microglial activation (Figures 2A and 2B), microglia cells were assessed. Consistent with our previous findings,[5] there was an increase in microglia cells at 4 weeks after CPB (Figures 5E and 5F). Notably, BM-MSC infusion inhibited the CPB-induced prolonged microglia increase (Figures 5E and 5F). We also found differences in microglia morphology such as terminal points and process length (Supplemental Figures 15A to 15C), demonstrating that BM-MSC treatment inhibits not only acute but also prolonged CPB-induced microglial activation. There was a correlation between microglia number and cortical FA values ($P = 0.036$), suggesting possible contributions of microglia expansion and neuroinflammation to microstructural alterations in the frontal cortex. Altogether, our studies demonstrate that MSC-induced inhibition of acute microglia activation and neuronal apoptosis subsequently limits prolonged microglia activation after CPB and improves structural alterations of the developing brain resulting from cardiac surgery.

EXOSOMAL microRNA miR-21-5P MAY BE A KEY DRIVER OF THE ANTIAPOPTOTIC AND ANTI-INFLAMMATORY EFFECTS OF BM-MSCs. BM-MSCs are known to mediate most of their beneficial effects through paracrine factors, which is consistent with our

FIGURE 6 Exosomal miRNAs Play a Prominent Role in the Beneficial Effects

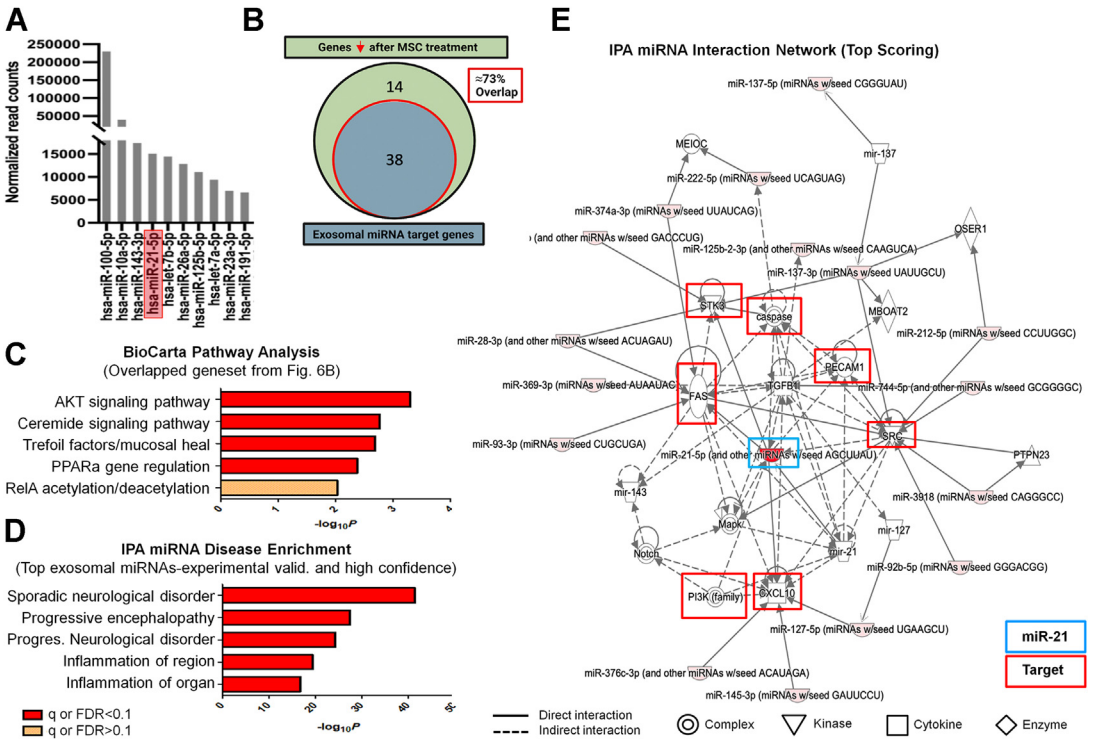

(A) Top 10 miRNAs by abundance in exosomes isolated from BM-MSCs including miR-21-5p (highlighted). (B) Overlap between down-regulated genes in piglet cortex following BM-MSC treatment obtained from the RNA sequencing experiment described in **Figure 3** (green) and the predicted target genes of miRNAs sequenced from BM-MSC exosomes (blue). More than 70% of genes found down-regulated in piglet cortex after BM-MSC treatment overlap with the target genes of exosomal miRNAs. (C) The overlapped gene set is enriched for genes implicated in the PI3K/AKT pathway. (D) MSC exosomal miRNAs are strongly associated with neurologic disorder and inflammation terms. (E) IPA miRNA-target interaction network analysis shows miR-21-5p as being uniquely associated with both PI3K/AKT and caspase signaling. BM-MSC = bone marrow–derived mesenchymal stromal cell; FDR = false discovery rate; IPA = Ingenuity Pathway Analysis; miRNA = microRNA; w = with.

findings of no long-term residual BM-MSCs (**Figure 4A**). Exosomes derived from BM-MSCs contain various microRNAs (miRNAs) that exert paracrine effects on surrounding cells and tissues.[36] To assess the contribution of exosomal miRNA species, we isolated BM-MSC exosomes, followed by RNA extraction and small RNA sequencing (Supplemental Figure 16A). Isolated exosomes were profiled by size and number (Supplemental Figures 16B and 16C). Among 423 miRNAs detected, the 10 most abundant exosomal miRNAs included miR-100-5p, miR-10a-5p, miR-143-3p, miR-21-5p, and let-7b-5p (**Figure 6A**).

To understand how these miRNAs may be related to the transcriptional changes seen in the piglet cortex after BM-MSC delivery (**Figure 3D**), we used Ingenuity Pathway Analysis (IPA) to obtain miRNA predicted target genes. When experimentally validated and high-scoring predicted targets were overlapped with the BM-MSC-treated piglet cortex down-regulated gene set, all target genes of the exosomal miRNAs were found in the host tissue DEG dataset (**Figure 6B**). More than 70% of genes identified as down-regulated in the cortex following BM-MSC treatment overlapped with the predicted target genes of miRNAs sequenced from BM-MSC exosomes (**Figure 6B**), indicating that exosomal miRNAs might play a prominent role in the transcriptional suppression induced by BM-MSCs. The overlapping genes were enriched for PI3K/AKT and ceramide signaling (**Figure 6C**), with 2 down-regulated genes (*Bad*, *Nfkbia*) accounting for the AKT enrichment term. These transcriptional changes are consistent with inhibited apoptosis initiation and an active NF-κB pathway signature (**Figures 3D and 3E**). To further

characterize the exosomal miRNAs, we used IPA to assess disease associations with altered miRNA expression. Notably, the exosomal miRNAs were identified as enriched for both sporadic and progressive neurologic disorder functional terms, as well as inflammation (**Figure 6D**, Supplemental Tables 5 and 6). Together, our results suggest that BM-MSC exosomal miRNAs are important in modulating neuroinflammatory processes that we observed in the cortical tissues post-BM-MSC delivery.

To map our dataset to known signaling pathways, we used the exosomal miRNAs as terms to construct interaction networks in IPA and identified a total of 26 network clusters (Supplemental Figure 17). Within the 26 clusters identified, 2 exosomal miRNAs, miR-21-5p and miR-143-3p, were identified as significant hub nodes in 7 interaction networks. Notably, miR-21-5p was involved in 6 high-scoring clusters as a significant network hub (Supplemental Figure 17). Our network analysis showed that miR-21-5p indirectly interacts with PI3K/AKT, caspase, and FAS terms (**Figure 6E**). Furthermore, the miR-21-5p seed sequence was found to align with both *STAT3* and *IL6ST* gene 3′ untranslated regions (Supplemental Figure 18), suggesting its importance in modulating PI3K/AKT signaling and the extrinsic apoptotic pathway via STAT3 signaling modulation. The essential role of miR-21-5p has been identified in exosome-mediated tissue repair.[37] Because miR-21-5p is highly expressed in BM-MSC exosomes (**Figure 6A**), our results suggest miR-21-5p as a potential molecular mediator of the beneficial effects of BM-MSCs on unique brain insults resulting from pediatric cardiac surgery.

DISCUSSION

This study using our piglet model identifies CPB as a safe and efficient administration system for BM-MSC delivery into the developing brain. In the cortex, BM-MSCs reduce microglial increase and shift their phenotype to a less proinflammatory state. Our analyses indicate JAK-STAT3 signaling as a possible molecular target for ameliorating inflammatory stress caused by CPB. BM-MSCs can inhibit CPB-induced microglial STAT3 overactivation and proapoptotic transcriptional signatures and limit neuronal apoptosis. Notably, BM-MSC treatment improves postoperative recovery and mitigates behavioral alterations resulting from CPB. Furthermore, our studies indicate a suppression of CPB-induced cortical microstructural abnormalities by BM-MSCs, possibly through the reduction of prolonged microglia activation. Finally, our transcriptomic analyses suggest that BM-MSC exosome-derived miRNAs such as miR-21-5p may be the key drivers of suppressed apoptosis and STAT3-mediated microglial activation observed following BM-MSC infusion, suggesting potential mechanisms underlying the therapeutic actions of BM-MSCs in brain insults after CPB.

MIGRATION DYNAMICS OF BM-MSCs DELIVERED THROUGH CPB AND THEIR PARACRINE FUNCTIONS. In this study, an MRI-based cell-tracking technique with SPIO nanoparticles allowed us to define the migration dynamics of BM-MSCs delivered through CPB and found that approximately half of BM-MSCs were localized to parenchyma shortly after CPB. We have previously identified disruption of the blood-brain barrier and an increase in its permeability after CPB.[38] In addition to the extravasation capacity of BM-MSCs,[9] CPB-induced alterations in blood-brain barrier function may uniquely contribute to the acute parenchymal localization of delivered BM-MSCs. Similar to our findings, intra-arterial infusion of BM-MSCs in rodents resulted in immediate cell localization to the injury site.[16] In the study, most cells disappeared during the next 24 hours.[16] We also observed no long-term residual BM-MSCs in the brain at postoperative week 4. Although the regenerative capacity of BM-MSCs has been overstated because of previous claims of BM-MSCs behaving as pluripotent stem cells in vivo to replace lost cells, their unique trophic properties have been well recognized.[9,11] Our findings support paracrine functions playing a major role in the beneficial effects of BM-MSCs. Indeed, our assays suggest that exosomal miRNAs derived from BM-MSCs account for their therapeutic actions in CPB-induced cortical injury. Future studies using this model should address the potential of MSC-derived vesicle treatment containing specific miRNAs like miR-21-5p as possible targeted CPB therapeutics.

POSSIBLE EFFECTS ON OTHER ORGANS. Our imaging study demonstrates diffuse distribution of BM-MSCs to multiple organs. The broad impact of CPB-induced oxidative and inflammatory stress is well recognized in various tissues.[4] Thus, additional studies are required to determine cellular/molecular events in other tissues after BM-MSC delivery.

MSC-INDUCED IMPROVEMENT OF BEHAVIORAL ALTERATION RESULTING FROM CARDIAC SURGERY. In addition to improvement of structural alterations, we found that BM-MSC treatment mitigates altered exploratory behaviors resulting from cardiac surgery. Behavioral problems and cortical dysmaturation are widespread among children with CHD.[1,3] Thus, the present study may contribute to the development of a new therapy for neuroprotection in the CHD

population. On the other hand, neurologic deficits associated with CHD are not simply a consequence of surgery and exposure to CPB but are multifactorial.[1,3] Because of the multietiologic nature, a combination of various treatments including the proposed BM-MSC treatment will be required to prevent adverse neurodevelopmental outcomes in children with CHD.

STUDY LIMITATIONS. Because piglets share many metabolic and physiologic similarities with humans, the use of piglets is highly translational. Limited genetic tools, however, prevent an in-depth investigation of causality in our findings, including the relationship of microglial activation to neuronal apoptosis as well as alteration in cortical microstructure. The limited availability of surface markers also inhibits distinguishing cell types and confirming findings from RNA sequencing. For instance, $Iba1^{+}CD11b^{+}$ cells may include macrophages that have entered the brain after CPB. Similarly, involvement of the pathways suggested by our transcriptomic analysis is correlative. Our mechanistic experiments were also performed in silico. Future experimental validation of these in silico target pathways would provide conclusive evidence for their role in the therapeutic effects of BM-MSCs. All RNA sequencing experiments in this study were performed in cortical tissues exposed to CPB using deep hypothermic circulatory arrest together with clinically used pump prime including corticosteroids. Thus, a different CPB strategy may result in different gene expression profiles from the ones observed. Although we conducted a well-controlled procedure in piglets, a small sample size because of logistical and ethical restrictions is another limitation. It is possible that the small numbers contributed to the lack of difference between groups in neuronal complexity. Similarly, a sham surgery group was not added in this study using piglets. Common surgery-induced insults such as anesthesia and/or thoracotomy may affect some of our findings. Brain injuries associated with pediatric cardiac surgery are multietiologic. Future studies will be necessary to distinguish each factor individually from the global impact of cardiac surgery. The present study used the open field test for behavioral assessments in the model. However, unlike in rodents, region-specific neurobehavioral assays have not been established in piglets. Further development of sophisticated behavior tests will be required for improvement of this unique model.

CONCLUSIONS

BM-MSC delivery through CPB has significant translational potential for minimizing inflammatory stress, microglial activation, and neuronal apoptosis during CPB, with subsequent inhibition of behavioral and structural deficits in children undergoing cardiac surgery. Our porcine model has given us insights into the therapeutic actions that explain antiapoptotic and anti-inflammatory processes occurring after BM-MSC treatment during CPB. Given the abundant evidence of neuroprotective capacities of BM-MSCs and their excellent safety record, successful completion of a phase 1 trial will be required to design new cell-based approaches for the improvement of neurodevelopmental impairment in children with CHD.

ACKNOWLEDGMENTS The authors would like to thank Dr Gary Stinnett for assistance with BM-MSC labeling, Christopher Liu for assistance with neuroimage quantification, Alice Chen and Julia Ryan for assistance with immunohistochemistry, Karuna Panchapakesan for assistance with cytokine/chemokine analysis, Dr Toru Sasaki and Payal Banerjee for their assistance with RNA sequencing, Krystal Grecco for assistance with positron emission tomography imaging, Robert Ulrey and Anushree Datar for immunophenotyping of BM-MSC products, and Bobbi K. Lewis for her support in MRI. The graphical abstract was created with BioRender.com. The authors are thankful for the generosity of the Foglia and Hill families who supported our studies.

FUNDING SUPPORT AND AUTHOR DISCLOSURES

This work was supported by National Institutes of Health (NIH) grants R01HL139712 (Dr Ishibashi), R01HL146670 (Dr Ishibashi), R21NS127051 (Dr Ishibashi) and NIMHHD U54MD007597 (Dr Wang) and by the Office of the Assistant Secretary of Defense for Health Affairs through the Peer Reviewed Medical Research Program under award no. W81XWH2010199 (Dr Ishibashi). The Clinical and Translational Science Institute was supported through NIH UL1TR001876 and KL2TR001877. District of Columbia Intellectual and Developmental Disabilities Research Center (DC-IDDRC) cores were supported by NIH U54HD090257. The content is solely the responsibility of the authors and does not necessarily represent the official views of the NIH, U.S. Department of Defense, or DC-IDDRC. Dr Hanley is a cofounder and on the Board of Directors of Mana Therapeutics, is on the Scientific Advisory Board of Cellevolve, and is an advisor to Maxcyte. All other authors have reported that they have no relationships relevant to the contents of this paper to disclose.

ADDRESS FOR CORRESPONDENCE: Dr Nobuyuki Ishibashi, Children's National Hospital, 111 Michigan Avenue, NW, Washington, DC 20010-2970, USA. E-mail: nishibas@childrensnational.org.

PERSPECTIVES

COMPETENCY IN MEDICAL KNOWLEDGE: Many children with congenital heart disease experience significant neurologic impairment; however, few treatment options are available. Oxidative stress and systemic inflammation during cardiac surgery remain major pathologic events in the neonatal and infant brain.

TRANSLATIONAL OUTLOOK: Delivery of mesenchymal stromal cells via cardiopulmonary bypass minimizes inflammatory stress and reduces microglial activation and neuronal apoptosis, with subsequent inhibition of cortical dysmaturation and behavioral alteration in our translational preclinical model. Successful completion of a phase 1 trial will be required to design new cell-based approaches for the improvement of neurodevelopmental impairment in children with congenital heart disease.

REFERENCES

1. Marelli A, Miller SP, Marino BS, Jefferson AL, Newburger JW. Brain in congenital heart disease across the lifespan: the cumulative burden of injury. *Circulation*. 2016;133:1951–1962.

2. Gaynor JW, Stopp C, Wypij D, et al. Neurodevelopmental outcomes after cardiac surgery in infancy. *Pediatrics*. 2015;135:816–825.

3. Morton PD, Ishibashi N, Jonas RA. Neurodevelopmental abnormalities and congenital heart disease: insights into altered brain maturation. *Circ Res*. 2017;120:960–977.

4. Zakkar M, Guida G, Suleiman MS, Angelini GD. Cardiopulmonary bypass and oxidative stress. *Oxid Med Cell Longev*. 2015;2015:189863.

5. Korotcova L, Kumar S, Agematsu K, Morton PD, Jonas RA, Ishibashi N. Prolonged white matter inflammation after cardiopulmonary bypass and circulatory arrest in a juvenile porcine model. *Ann Thorac Surg*. 2015;100:1030–1037.

6. Dhari Z, Leonetti C, Lin S, et al. Impact of cardiopulmonary bypass on neurogenesis and cortical maturation. *Ann Neurol*. 2021;90:913–926.

7. Beca J, Gunn JK, Coleman L, et al. New white matter brain injury after infant heart surgery is associated with diagnostic group and the use of circulatory arrest. *Circulation*. 2013;127:971–979.

8. Rettenmaier LA, Kirby PA, Reinking BE, Viaene AN, Hefti MM. Neuropathology of congenital heart disease in an inpatient autopsy cohort 2000-2017. *J Am Heart Assoc*. 2020;9:e013575.

9. Uccelli A, Moretta L, Pistoia V. Mesenchymal stem cells in health and disease. *Nat Rev Immunol*. 2008;8:726–736.

10. van Velthoven CT, Kavelaars A, Heijnen CJ. Mesenchymal stem cells as a treatment for neonatal ischemic brain damage. *Pediatr Res*. 2012;71:474–481.

11. Eckert MA, Vu Q, Xie K, et al. Evidence for high translational potential of mesenchymal stromal cell therapy to improve recovery from ischemic stroke. *J Cereb Blood Flow Metab*. 2013;33:1322–1334.

12. Wagenaar N, Nijboer CH, van Bel F. Repair of neonatal brain injury: bringing stem cell-based therapy into clinical practice. *Dev Med Child Neurol*. 2017;59:997–1003.

13. Detante O, Moisan A, Dimastromatteo J, et al. Intravenous administration of 99mTc-HMPAO-labeled human mesenchymal stem cells after stroke: in vivo imaging and biodistribution. *Cell Transplant*. 2009;18:1369–1379.

14. Makinen S, Kekarainen T, Nystedt J, et al. Human umbilical cord blood cells do not improve sensorimotor or cognitive outcome following transient middle cerebral artery occlusion in rats. *Brain Res*. 2006;1123:207–215.

15. Walczak P, Wojtkiewicz J, Nowakowski A, et al. Real-time MRI for precise and predictable intra-arterial stem cell delivery to the central nervous system. *J Cereb Blood Flow Metab*. 2017;37:2346–2358.

16. Mitkari B, Kerkela E, Nystedt J, et al. Intra-arterial infusion of human bone marrow-derived mesenchymal stem cells results in transient localization in the brain after cerebral ischemia in rats. *Exp Neurol*. 2013;239:158–162.

17. Hanley PJ, Mei Z, Durett AG, et al. Efficient manufacturing of therapeutic mesenchymal stromal cells with the use of the Quantum Cell Expansion System. *Cytotherapy*. 2014;16:1048–1058.

18. Frank JA, Miller BR, Arbab AS, et al. Clinically applicable labeling of mammalian and stem cells by combining superparamagnetic iron oxides and transfection agents. *Radiology*. 2003;228:480–487.

19. Borlongan CV, Glover LE, Tajiri N, Kaneko Y, Freeman TB. The great migration of bone marrow-derived stem cells toward the ischemic brain: therapeutic implications for stroke and other neurological disorders. *Prog Neurobiol*. 2011;95:213–228.

20. Ishibashi N, Iwata Y, Okamura T, Zurakowski D, Lidov HG, Jonas RA. Differential neuronal vulnerability varies according to specific cardiopulmonary bypass insult in a porcine survival model. *J Thorac Cardiovasc Surg*. 2010;140:1408–1415.e3.

21. Ishibashi N, Scafidi J, Murata A, et al. White matter protection in congenital heart surgery. *Circulation*. 2012;125:859–871.

22. Moniche F, Gonzalez A, Gonzalez-Marcos JR, et al. Intra-arterial bone marrow mononuclear cells in ischemic stroke: a pilot clinical trial. *Stroke*. 2012;43:2242–2244.

23. Ghali AA, Yousef MK, Ragab OA, ElZamarany EA. Intra-arterial infusion of autologous bone marrow mononuclear stem cells in subacute ischemic stroke patients. *Front Neurol*. 2016;7:228.

24. Nayak D, Roth TL, McGavern DB. Microglia development and function. *Annu Rev Immunol*. 2014;32:367–402.

25. Chen S, Dong Z, Cheng M, et al. Homocysteine exaggerates microglia activation and neuroinflammation through microglia localized STAT3 overactivation following ischemic stroke. *J Neuroinflammation*. 2017;14:187.

26. Zheng ZV, Chen J, Lyu H, et al. Novel role of STAT3 in microglia-dependent neuroinflammation after experimental subarachnoid haemorrhage. *Stroke Vasc Neurol*. 2022;7:62–70.

27. Springer JE, Azbill RD, Knapp PE. Activation of the caspase-3 apoptotic cascade in traumatic spinal cord injury. *Nat Med*. 1999;5:943–946.

28. Luo JL, Kamata H, Karin M. The anti-death machinery in IKK/NF-kappaB signaling. *J Clin Immunol*. 2005;25:541–550.

29. Li H, Chen Z, Zhou S. Apoptosis in glioma-bearing rats after neural stem cell transplantation. *Neural Regen Res*. 2013;8:1793–1802.

30. Desole C, Gallo S, Vitacolonna A, et al. HGF and MET: from brain development to neurological disorders. *Front Cell Dev Biol*. 2021;9:683609.

31. Salter MW, Stevens B. Microglia emerge as central players in brain disease. *Nat Med*. 2017;23:1018–1027.

32. Wakselman S, Bechade C, Roumier A, Bernard D, Triller A, Bessis A. Developmental neuronal death in hippocampus requires the microglial CD11b integrin and DAP12 immunoreceptor. *J Neurosci*. 2008;28:8138–8143.

33. Giunti D, Parodi B, Usai C, et al. Mesenchymal stem cells shape microglia effector functions through the release of CX3CL1. *Stem Cells*. 2012;30:2044–2053.

34. Dean JM, McClendon E, Hansen K, et al. Prenatal cerebral ischemia disrupts MRI-defined cortical microstructure through disturbances in neuronal arborization. *Sci Transl Med*. 2013;5:168ra7.

35. Budde MD, Janes L, Gold E, Turtzo LC, Frank JA. The contribution of gliosis to diffusion tensor anisotropy and tractography following traumatic brain injury: validation in the rat using Fourier analysis of stained tissue sections. *Brain*. 2011;134:2248–2260.

36. Phinney DG, Pittenger MF. Concise review: MSC-derived exosomes for cell-free therapy. *Stem Cells*. 2017;35:851–858.

37. Qiao L, Hu S, Liu S, et al. microRNA-21-5p dysregulation in exosomes derived from heart failure patients impairs regenerative potential. *J Clin Invest*. 2019;129:2237–2250.

38. Okamura T, Ishibashi N, Kumar TS, et al. Hypothermic circulatory arrest increases permeability of the blood brain barrier in watershed areas. *Ann Thorac Surg*. 2010;90:2001–2008.

KEY WORDS cardiac surgery, cardiopulmonary bypass, congenital heart disease, mesenchymal stromal cells, neuroprotection

APPENDIX For an expanded Methods section as well as supplemental tables and figures, please see the online version of this paper.